# DAB2IP Is a Bifunctional Tumor Suppressor That Regulates Wild-Type RAS and Inflammatory Cascades in KRAS Mutant Colon Cancer

Abigail L. Miller[1,2], Naiara Perurena[1,2], Alycia Gardner[1,2], Toshinori Hinoue[3], Patrick Loi[1,2], Peter W. Laird[3], and Karen Cichowski[1,2]

## ABSTRACT

The *DAB2IP* tumor suppressor encodes a RAS GTPase-activating protein. Accordingly, DAB2IP has been shown to be mutated or suppressed in tumor types that typically lack RAS mutations. However, here we report that *DAB2IP* is mutated or selectively silenced in the vast majority of *KRAS* and *BRAF* mutant colorectal cancers. In this setting, DAB2IP loss promoted tumor development by activating wild-type H- and N-RAS proteins, which was surprisingly required to achieve robust activation of RAS effector pathways in *KRAS*-mutant tumors. *DAB2IP* loss also triggered production of inflammatory mediators and the recruitment of protumorigenic macrophages *in vivo*. Importantly, tumor growth was suppressed by depleting macrophages or inhibiting cytokine/inflammatory mediator expression with a JAK/TBK1 inhibitor. In human tumors, *DAB2IP* was lost at early stages of tumor development, and its depletion was associated with an enrichment of macrophage and inflammatory signatures. Together, these findings demonstrate that DAB2IP restrains the activation of the RAS pathway and inflammatory cascades in the colon and that its loss represents a common and unappreciated mechanism for amplifying these two critical oncogenic signals in colorectal cancer.

**Significance:** *DAB2IP* is lost in early-stage tumors, which amplifies RAS signaling, triggers inflammatory mediators, and recruits macrophages in *KRAS*-mutant colon cancers.

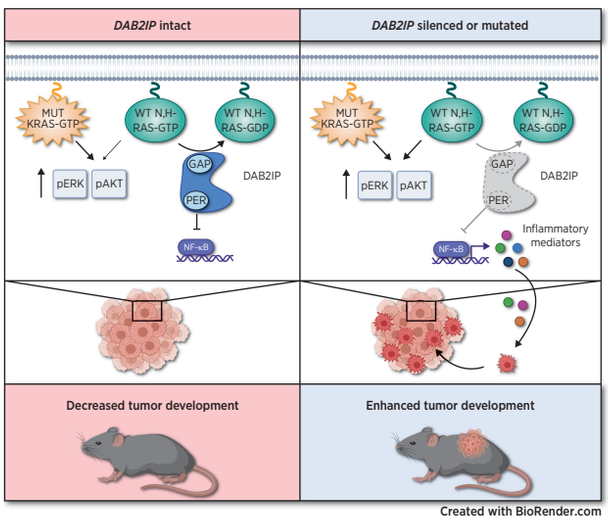


## Introduction

The RAS pathway is one of the most commonly deregulated signaling pathways in human cancer, with nearly 30% of tumors harboring a mutation in one of the *RAS* genes (1). Activating mutations in *KRAS* are particularly common in colorectal cancers and arise in approximately 40% of tumors, whereas *BRAF* mutations are more prevalent in high-level microsatellite instability (MSI-high) lesions (2). Regardless, genomic studies and mouse modeling efforts suggest that aberrant activation of the RAS pathway is an important and relatively early oncogenic event in colorectal cancer development (3–7).

In addition to genetic alterations, inflammation also contributes to the development of colorectal cancer (8). For example, inflammatory bowel diseases (IBD) such as ulcerative colitis and Crohn's disease promote the development of colitis-associated colon cancers (9). Conversely, NSAIDs broadly decrease the incidence of colorectal cancer (10, 11). The process of inflammation is mediated by cytokines and chemokines produced by tumor cells and by cells recruited to the tumor microenvironment (TME; ref. 12). Notably, the reciprocal communication between cell types within a tumor is required to amplify cytokine signaling pathways and establish an inflammatory environment (8). However, while IBD, infections, and other environmental factors are known to trigger inflammation in the colon, only 5% of tumors develop as a consequence of overt chronic inflammation caused by these events (8). Much less is known about how tumor cells themselves may initiate cytokine-driven inflammatory cascades. Mutations affecting the WNT and p53 pathways have been shown to impair intestinal barrier function, which can indirectly enhance cytokine/chemokine signaling cascades triggered by microbes; however, it is not known whether or how genetic/epigenetic defects in colorectal cancer cells may directly initiate cytokine-mediated communication with the TME (13, 14).

We began this study by exploring a broader role for the *DAB2IP* tumor suppressor in human cancer. *DAB2IP* encodes a RAS GTPase-activating protein (RASGAP), which normally turns off RAS by

[1]Genetics Division, Department of Medicine, Brigham and Women's Hospital, Boston, Massachusetts. [2]Harvard Medical School, Boston, Massachusetts. [3]Van Andel Institute, Grand Rapids, Michigan.

**Corresponding Author:** Karen Cichowski, 77 Avenue Louis Pasteur, NRB 0458D, Boston, MA 02115. Phone: 617-525-4722; E-mail: kcichowski@rics.bwh.harvard.edu

Cancer Res 2023;83:1800–14

**doi:** 10.1158/0008-5472.CAN-22-0370

catalyzing the hydrolysis of Ras-GTP (15). Given its RASGAP function, we expected that *DAB2IP* would be mutated or lost primarily in malignancies lacking mutations in *RAS* and *RAF* genes, thereby providing an alternative means of activating the RAS pathway in these tumors. Surprisingly however, we found that *DAB2IP* is most frequently mutated/suppressed in colorectal cancers and is inactivated in the vast majority of tumors harboring *KRAS* or *BRAF* mutations. In this study, we show that DAB2IP plays such an important role in colon cancer because it both dramatically amplifies RAS signaling, even in *KRAS*-mutant tumors, and potently triggers the production of inflammatory mediators and the recruitment of protumorigenic macrophages. Together these studies reveal a common and unappreciated mechanism by which the RAS pathway and inflammatory cascades are amplified early in the development of colorectal cancer.

## Materials and Methods

### Animals

#### Human colon cancer cell line–derived xenograft models

Animal procedures were approved by the Center for Animal and Comparative Medicine at Harvard Medical School in accordance with the NIH Guide for the Care and Use of Laboratory Animals and the Animal Welfare Act. Cancer cell line–derived xenograft experiments were performed in 6- to 10-week-old female Nu/Nu mice purchased from Charles River Laboratories. The same procedure outlined below was used for each cell line–derived xenograft experiment. Cells were tested for *Mycoplasma* before injection into the flank of mice. Additional information about the generation of the models is noted below.

### Cell lines

Human colon cancer cell lines CACO2 (catalog no. HTB-37, RRID: CVCL_0025), DLD-1 (catalog no. CCL-221, RRID:CVCL_0248), HCT15 (catalog no. CCL-225, RRID:CVCL_0292), HCT116 (catalog no. CCL-247, RRID:CVCL_0291), HT29 (catalog no. HTB-38, RRID: CVCL_0320), LOVO (catalog no. CCL-229, RRID:CVCL_0399), LS411N (catalog no. CRL-2159, RRID:CVCL_1385), RKO (catalog no. CRL-2577, RRID:CVCL_0504), SW480 (catalog no. CCL-228, RRID:CVCL_0546), SW1417 (catalog no. CCL-238, RRID:CVCL_ 1717), and mouse macrophages RAW 264.7 (catalog no. TIB-71, RRID:CVCL_0493) were purchased from the ATCC. KM12 (RRID: CVCL_1331), OUMS23 (RRID:CVCL_3088), and SW48 (RRID: CVCL_1724) human colon cancer cell lines were kind gifts from W. Hahn. These cell lines were authenticated using short tandem repeat profiling (Labcorp). KM12 cells did contain extra peaks next to the main markers exhibited by MSI-high cell lines. CACO2, KM12, OUMS23, RKO, SW480, and SW1417 cells were cultured in DMEM media. DLD-1, HCT15, LS411N, and LOVO cells were cultured in RPMI media. HCT116 and HT29 cells were cultured in McCoy's 5A media. Human embryonic kidney 293T (catalog no. CRL-3216, RRID: CVCL_0063) cells were cultured in DMEM media. All media were supplemented with 10% FBS and 2 mmol/L glutamine (Gibco, catalog no. 25030081) and cells were cultured at 37°C under 5% $CO_2$. Cell lines were tested to confirm lack of *Mycoplasma* contamination.

### Plasmids and siRNAs

The following plasmids were used: pFB NEO LACZ, DAB2IP, R289L, and S604A, which were previously described (16). LACZ, DAB2IP, R289L, and S604A were also cloned into the pHAGE-C-Flag-HA lentiviral expression vector (Dr. J. Wade Harper, Harvard Medical School, Boston, MA).

For knockdown experiments, 3′-UTR DAB2IP short hairpin RNA (shRNA; 5′- GTAATGTAACTATCTCACCTA −3′) and a control shRNA (5′-CCTAAGGTTAAGTCGCCCTCG-3′) were used as previously described (16). 3′-UTR shDAB2IP and control shRNA were also cloned into PLKO.1 blasticidin (Addgene, catalog no. 26655). siControl and siDAB2IP were purchased from Dharmacon (ON-TARGETplus Non-targeting Control Pool, catalog no. D-001810–10, and SMARTpool HUMAN siGENOME DAB2IP, catalog no. #L-008249–01: 5′-CGCAGUUGUUAGAAGACGA-3′ / 5′-GGCUAAG-GAGUAAGGACGA-3′ / 5′-GGACCAACAUGCAGCGCUU-3′ / 5′-GAUAGAUUUCACCCGGUUA-3′).

For the NF-κB assays, pNF-κB luciferase and pRL-TK (RRID: Addgene_11313), or pGL4.70 [*hRluc*] (Promega, catalog no. E6881) are the reporter plasmids used (17). pBABE puro (RRID: Addgene_21836; control), pBABE IκBα super repressor puro (RRID:Addgene_15291) or IκBα super repressor cloned into pBABE neomycin (RRID:Addgene_1767) were used as inhibitors of NF-κB signaling.

### Western blotting

Cells were lysed in boiling 1% SDS lysis buffer (10 mmol/L Tris pH 7.5, 100 mmol/L NaCl, 1% SDS), scraped into a tube, and boiled for 10 to 15 minutes. Lysates were centrifuged for 10 minutes before performing a Pierce BCA protein assay (Thermo Fisher, catalog no. 23225) for protein normalization. 15 to 30 μg of lysate was loaded onto 8% or 12% SDS-PAGE mini gels and transferred onto polyvinylidene difluoride membranes. Membranes were blocked for 1 hour with 5% milk in TBST buffer and incubated overnight at 4°C with primary antibodies. The following antibodies were used at the indicated dilutions in the blocking buffer: DAB2IP (Abcam, catalog no. ab87811, RRID:AB_2041032) 1:2500, DAB2IP (Santa Cruz Biotechnology, catalog no. sc-365921, RRID:AB_10917204) 1:1,000, α-TUBULIN (Sigma, catalog no. T5168, RRID:AB_477579) 1:10,000, VINCULIN (Cell Signaling Technology, catalog no. 4650, RRID:AB_10559207) 1:1,000, pERK (Cell Signaling Technology, catalog no. 4370, RRID:AB_2315112) 1:2,000, ERK (Cell Signaling Technology, catalog no. 9102, RRID:AB_330744) 1:3,000, pAKT (Cell Signaling Technology, catalog no. 4060, RRID:AB_2315049) 1:1,000, AKT (Cell Signaling Technology, catalog no. 9272, RRID: AB_329827) 1:2,000, GAPDH (Cell Signaling Technology, catalog no. 2118, RRID:AB_561053) 1:5,000, H-RAS (Santa Cruz Biotechnology, catalog no. sc-520, RRID:AB_631670) 1:500, K-RAS (Santa Cruz Biotechnology, catalog no. sc-30, RRID:AB_627865) 1:200, N-RAS (Santa Cruz Biotechnology, catalog no. sc-519, RRID: AB_632073) 1:200, IκBα (Santa Cruz Biotechnology, catalog no. sc-371, RRID:AB_2235952) 1:1,000, p-P65 (Cell Signaling Technology, catalog no. 3033, RRID:AB_331284) 1:1,000, P65 (Abcam, catalog no. ab7970, RRID:AB_306184) 1:2,000, MCL1 (Cell Signaling Technology, catalog no. 39224, RRID:AB_2799149) 1:1,000, BCL-XL (Cell Signaling Technology, catalog no. 2764, RRID:AB_2228008) 1:1,000, BCL2 (Cell Signaling Technology, catalog no. 4223, RRID:AB_1903909) 1:1,000, TRAF1 (Cell Signaling Technology, catalog no. 4715, RRID:AB_2303912) 1:1,000, TRAF2 (Cell Signaling Technology, catalog no. 4724, RRID: AB_2209845) 1:1,000, CIAP1 (Cell Signaling Technology, catalog no. 7065, RRID:AB_10890862) 1:1,000, CIAP2 (Cell Signaling Technology, catalog no. 3130, RRID:AB_10693298) 1:1,000, XIAP (Proteintech, catalog no. 10037–1-Ig, RRID:AB_2215009) 1:1,000, C-FLIP (Proteintech, catalog no. 10394–1-AP, RRID:AB_2081087) 1:1,000.

### Cell proliferation assays

For each sample, $1.5 \times 10^4$ cells were seeded per well in a 12-well plate. Technical triplicates were used for each sample. Cells were counted the following day (day 0), and every 24 hours after for the next 3 days. Each day counts were compared with day 0 counts to determine the change in cell number. At least three biological replicates were performed with representative experiments with technical triplicates shown.

### Soft agar assays

Six-well plates were coated with 0.5% (w/v) agarose in cell culture media. For each sample, $1 \times 10^3$ to $1 \times 10^4$ cells were suspended in 0.375% (w/v) agarose in cell culture media supplemented with 1% streptomycin/penicillin and plated in 1 well. Technical triplicates were used for each sample. Plates were fed every 2 weeks for 3 to 6 weeks. Cells were fixed with 2% paraformaldehyde for 30 minutes and stained with 0.0005% (w/v) crystal violet. Plates were scanned and quantified using ImageJ (ImageJ, RRID:SCR_003070). At least three biological replicates were performed for each experiment.

### Ras-GTP assays

Ras-GTP levels were measured using a RAS Activation Assay Kit (Millipore Sigma, catalog no. 17–218). Cells were plated at 80% to 90% confluency. The following day, cells were lysed with 1X Mg2+ Lysis/Wash Buffer in 10% glycerol supplemented with EDTA-free protease inhibitor tablets and 25 mmol/L sodium fluoride and 1-mmol/L sodium orthovanadate. 750 to 1,500 μg of lysate was incubated with 10 μg of Raf-1 RBD, agarose for 2 hours rotating at 4°C. Samples were washed 3 times with lysis buffer and resuspended in 2x sample loading buffer (100 mmol/L Tris pH 6.8, 10% glycerol, 3.5% SDS, 10% DTT, 0.4% bromophenol blue). Whole cell lysates and GTP assays were boiled and run on 12% SDS-PAGE gels. The antibodies for Western blot analysis are listed above.

### NF-κB luciferase assay

For each sample, $2 \times 10^5$ to $3.5 \times 10^5$ cells per well or $1 \times 10^6$ (LOVO only) were plated in a 6-well plate. The following day stably expressed cells lines (cDNA or shRNA) were transfected with 1 μg of pNF-κB luciferase (17) and 250 ng of *Renilla* luciferase encoding plasmid (pRL-TK) or 500 ng of pGL4.70 [hRluc]. For DLD-1 and LOVO experiments, cells were cotransfected with the same concentration of reporter plasmids and 1 μg of LACZ (CNT) or DAB2IP (D2) cDNA. The following day, the transfected cells were plated into 3 wells each of a 24-well plate. Twenty-four hours after transfection, cells were stimulated with 20 ng/mL TNFα (Sigma, catalog no. T-0157–10UG). Three or 6 hours after TNFα treatment cells were washed and lysed. Luciferase activity was measured followed by *Renilla* luciferase activity using the Dual Luciferase Reporter Assay Kit (Promega, catalog no. E1910). All data were normalized as relative luciferase light units/*Renilla* luciferase light units. At least three biological replicates were performed.

### RNA sequencing

DLD-1 cells were infected with FB LACZ or FB DAB2IP and subsequently selected in neomycin. 7 days later, $5 \times 10^5$ cells were plated in triplicate in 6-well plates. RNA was harvested 2 days later using RNeasy Plus kit (Qiagen, catalog no. 74134). RNA was sequenced at Dana-Farber Cancer Institute Molecular Biology Core Facility using the Illumina NextSeq500. Raw data was mapped to the Hg19 genome using STAR (RRID:SCR_004463) and count files were made using HTSeq48,49 (GEO ID GSE224869). HCT116 cells were infected with shCNT or shDAB2IP and subsequently selected with puromycin. Seven days later, $5 \times 10^5$ cells were plated in triplicate in 6-well plates. RNA was harvested 2 days later using RNeasy Plus kit (Qiagen, catalog no. 74134). RNA was sequenced by Novogene (GEO ID GSE224870).

### Gene set enrichment analysis

We analyzed the mRNA expression from the colorectal cancer dataset from The Cancer Genome Atlas (TCGA) PanCan Atlas project (18), comparing the highest and lowest expressing DAB2IP samples of the 592 samples ($n = 30$ each). The data_mrna_seq_v2_rsem.txt file was downloaded from cBioPortal (RRID:SCR_014555; http://www.cbioportal.org/study/summary?id=coadread_tcga_pan_can_atlas_2018). Single-sample gene set enrichment analysis (ssGSEA) was performed with GenePattern (RRID:SCR_003201) using the following gene set from the Molecular Signatures Database (RRID:SCR_016863): HINATA_NFK-B_IMMU_INF (19). For HCT116 sh*CT* and sh*DAB2IP* cells, FKPM counts were used from RNA sequencing (RNA-seq). For DLD-1 *LACZ* (CNT) and *DAB2IP* cells, TPM counts were used. For macrophage enrichment in DAB2IP low tumors, ssGSEA was performed using a macrophage transcriptional profile (Supplementary Table S1; ref. 20) and plotted.

### DNA methylation data

We analyzed the colorectal cancer dataset from TCGA project, including 353 tumors and 32 adjacent nonmalignant tissues profiled using the Infinium HumanMethylation450 (HM450) array (18). IDAT files were downloaded from the NCI Genomic Data Commons (GDC) Portal (RRID:SCR_014514; ref. 20) and processed using *openSeSAMe* (RRID:SCR_002849) pipeline implemented in the R package *SeSA-Me* (21). The HM450 platform analyzes DNA methylation status of up to 482,421 CpG sites throughout the genome. It covers 99% of RefSeq genes with multiple probes per gene and 96% of CpG islands from the UCSC database and their flanking regions. The assay probe sequences and information for each interrogated CpG site on the platform are available at http://zwdzwd.github.io/InfiniumAnnotation (PMID: 27924034).

### Promoter DNA methylation analysis of RASGAPs genes

We investigated promoter DNA methylation status of 15 RASGAPs (Supplementary Table S2). For each gene, we selected CpG sites in the promoter region, defined as the 2 kb region spanning from 1,000 bp upstream to 1,000 bp downstream of the transcription start sites (TSS) based on GENCODE (release 22; GENCODE, RRID:SCR_014966; ref. 21), that were unmethylated in normal tissues (median β-value < 0.1 and β-value < 0.3 across all samples). We further selected one CpG site per gene showing the highest frequency of hypermethylation in the tumors. In the case of a tie, the CpG located closest to the TSSs was selected. Four genes were excluded from the heatmap analysis for the following reasons: Promoter probes for *RASA4* and *RASA4B* were masked owing to a problematic design issue (21). Promoter probes for *PLXNB2* and *RASAL3* were methylated in normal tissues based on the criteria above and were thus also excluded. Three tumors having any missing data for the remaining genes were omitted. Genes (rows) were arranged from top to bottom in order of decreasing hypermethylation frequency, and tumors (columns) were sorted to show overlap and mutual exclusivity of hypermethylation across tumors. The list of the probe IDs we selected is provided in Supplementary Table S2.

### *KRAS* mutation data

We obtained the MAF file generated for the TCGA PanCan Atlas project (22) and extracted *KRAS* mutation calls for the colorectal

tumors. *KRAS* mutations were grouped into four categories, G12, G13, Q61, and A146. Six tumors that had multiple mutations assigned in more than one category were excluded from the analysis.

### *DAB2IP* mutation analysis

The graph of *DAB2IP* mutations in different cancer tissues was created in cBioPortal (cbioportal, RRID:SCR_014555), using a curated set of nonredundant studies with a minimum of 50 total cases, excluding metastatic, PDX, and mixed tumor studies. *DAB2IP* mutations plotted along the *DAB2IP* gene were compiled from both cBioPortal and COSMIC (https://cancer.sanger.ac.uk/cosmic; COSMIC, RRID:SCR_014966) databases. Missense mutations were analyzed for functional impact using PolyPhen-2 (PolyPhen: Polymorphism Phenotyping, RRID:SCR_013189; ref. 23), an algorithm predicting the effects of an amino acid substitution on protein structure and function.

### *DAB2IP* expression analysis

To evaluate the expression of *DAB2IP* transcript variants, we obtained TCGA RNA-seq exon-quantification data from the NCI GDC Legacy Archive (https://portal.gdc.cancer.gov/legacy-archive). We analyzed RPKM values in 338 colorectal tumors and 15 adjacent nonmalignant tissues, for which the HM450 DNA methylation data were also available. RPKM values from exon (chr9:124522164–124522718 - GRCh37/hg19), shared by all four transcript variants in GENCODE (release 34), were plotted.

### Infections and transfections

shRNA or cDNA lentiviral or retroviral constructs were prepared, and virus was harvested as previously described (24). Virus was incubated on target cells twice, first for 6 hours and then for 16 hours to overnight at a 1:2 to 1:6 dilution with 8 μg/mL polybrene. The cells were allowed to recover for 24 hours before selection. Infected cells were selected in 2-μg/mL puromycin, 0.5 mg/mL geneticin (neomycin), or 5 to 10 μg/mL blasticidin, depending on the construct and optimized for each cell line. Selections continued until uninfected control plates were killed, approximately 1 to 4 days depending on the cell line.

For siRNA transfections, cells were transfected for 16 hours with 40 nmol/L siRNA using a 1:400 dilution of Lipofectamine RNAiMAX (ThermoFisher, catalog no. 13778–075) in media. ON-TARGETplus nontargeting control and human DAB2IP siRNA pools were used (Dharmacon, catalog no. D-001810–10 and L-008249–01).

### Human cancer cell xenograft models

For tumor formation studies, $1 \times 10^6$ cells in PBS were injected into the left and right flank of each mouse. Thus, each mouse contributed two tumors for each condition [shControl (shCT) and shDAB2IP] and (CNT, DAB2IP, R289L, S604A, IκBαSR) such that there were four mice and eight tumors per condition. Tumor size was measured every 2 to 3 days by calipers. Tumor volume was calculated using the standard formula $L \times W^2 \times 0.52$.

For the cytokine inhibitor study, $1 \times 10^6$ shDAB2IP cells in PBS were injected into the left and right flank of each mouse ($n = 16$), for a total of 32 injections. One day prior to cell implantation, mice were administered 50 mg/kg of CYT-387 (ChemieTek, catalog no. CT-CYT387) or vehicle [0.5% (w/v) hydroxypropyl methylcellulose (Sigma Aldrich, catalog no. H7509), 0.1% Tween 80, pH 8.0] by oral gavage. Treatment was administered daily. Tumor volume was calculated and graphed.

For the macrophage depletion study, $1 \times 10^6$ shDAB2IP cells in PBS were injected into the left and right flank of each mouse ($n = 37$), for a total of 74 injections. 3 days prior to cell implantation, mice were administered 1 mg of Chlodrosome or the control Encapsome (Encapsula NanoSciences, catalog no. CLD-8901) through intravenous tail vein injection. Treatment was administered every 3 days.

### Cytokine/inflammatory mediator analysis

For cells, (CNT and DAB2IP) were lysed in Lysis Buffer 17 (1% Igepal CA-630, 20 mmol/L Tris-HCl (pH 8.0), 137 mmol/L NaCl, 2 mmol/L EDTA, 200 mmol/L Sodium orthovanadate, 5 mmol/L NaF) supplemented with EDTA-free protease inhibitor tablets for 30 minutes on ice with gentle agitation. For tumors, 100 to 300 $mm^3$ tumors were analyzed. (shDAB2IP tumors) and (shDAB2IP tumors treated with vehicle or 50 mg/kg CYT-387 (ChemieTek, CT-CYT387) daily for 3 days and harvested 4 hours after the last treatment) were flash frozen, crushed, and homogenized in Tissue Lysis buffer (0.5% Igepal, 0.5% sodium deoxycholate, 0.1% SDS, 50 mmol/L Tris-HCl pH 7.5, and 150 mmol/L NaCl) supplemented with EDTA-free protease inhibitor tablets. Lysates were centrifuged and proteins were normalized. 400 to 500 μg were analyzed using Proteome Profiler Human Cytokine Array (R&D systems, catalog no. ARY005B). Membranes were imaged and quantified using ImageJ. All samples were performed in duplicate.

### Migration assay

shCT and shDAB2IP HCT116 cells were evenly plated in McCoy's 5A media (Corning, catalog no. 10–050-CV) containing 10% FBS and allowed to grow to 90% confluency (approximately 2 days in culture) to generate conditioned media. The conditioned media was collected and centrifuged at $1{,}000 \times g$ for 5 minutes to remove dead cells. For each well, 600 μL of the appropriate media was added to the bottom well, and each condition was plated in triplicate. A total of $2 \times 10^5$ RAW264.7 cells in 100 μL DMEM were added to the top well of the plate. Cells were allowed to migrate for 4 to 6 hours at 37°C and 5% $CO_2$. Following migration, cells remaining on the upper surface of the membrane were removed with cotton swabs, and inserts were incubated in 100% methanol for 10 minutes at −20°C to fix the migrated cells on the lower surface. Inserts were then stained in 0.2% crystal violet for 10 minutes at room temperature, washed 3 times in deionized water, and allowed to dry. Membranes were removed from the transwell insert and mounted on slides using Permount Mounting Medium (Fisher Scientific, catalog no. SP15–100). Membranes were imaged at ×10 magnification, with 5 random ROI selected for each membrane, and the migrating cells were manually counted. Three biological replicates were performed. One representative experiment with appropriate statistics is shown.

### IHC analysis

For xenograft tumors, $1 \times 10^6$ cells in PBS were injected into the left and right flank of each mouse. Tumors were harvested between 4 and 14 days post injection. For macrophages in the spleen, mice were administered 1 mg of Chlodrosome or the control Encapsome (Encapsula NanoSciences, catalog no. CLD-8901) through intravenous tail vein injection on day 1 and day 4. Spleens were harvested at day 5. All tissues were fixed in buffered formalin, stored in 70% ethanol, paraffin embedded, sectioned, and stained for hematoxylin and eosin where indicated. IHC was performed on the Leica Bond III automated staining platform using the Leica Biosystems Refine Detection Kit. For pERK staining, antibody Phospho-p44/42 MAPK (Erk1/2; Cell Signaling Technology, catalog no. 4370, RRID:AB_2315112) was run at a 1:150 dilution with citrate antigen retrieval. For F4/80 staining, anti-F4/80 (catalog no.

70076, RRID:AB_2799771) was run at a 1:500 dilution. Multiple tumor samples and spleens were analyzed.

### Quantification and statistical analysis

For quantitative measurements, graphs represent mean ± SD, apart from graphs with tumor volume data in which the mean ± SEM is represented. Where indicated data are presented as fold change over the control measurement. Two-tailed unpaired *t* tests, Mann–Whitney U tests, one-way ANOVA followed by Tukey multiple comparisons test, Fisher exact test, and Wilcoxon rank sum test were used to compare data sets where indicated, and *P* values marked with asterisks in the figures are listed with exact numbers in the figure legends. For Tukey boxplots, the interquartile range is represented with median line and outliers shown. A *P* value less than or equal to 0.05 was considered significant. Data were graphed in Excel or GraphPad Prism v.6 and statistically analyzed using GraphPad (GraphPad Prism, RRID:SCR_002798).

### Materials and data availability

All unique reagents generated in this study are available from the corresponding author and may require a completed Materials Transfer Agreement. RNA-seq data are available at GEO with IDs GSE224869 and GSE224870. The methylation and expression data are available in the NCI GDC Legacy Archive (https://portal.gdc.cancer.gov/legacy-archive). The expression dataset used for ssGSEA is available at cBioPortal (http://www.cbioportal.org/study/summary?id=coadread_tcga_pan_can_atlas_2018). All other raw data are available by request from the corresponding author.

## Results

### The *DAB2IP* tumor suppressor is frequently inactivated in human colorectal cancer via genetic and epigenetic mechanisms

The RASGAP gene, *DAB2IP*, has been shown to function as a tumor and metastasis suppressor in prostate and breast cancers (16, 25). To identify other tumor types in which *DAB2IP* loss might be important, we investigated the relative frequency of *DAB2IP* mutations using cBioPortal and COSMIC datasets. Mutations were observed in a variety of human cancers with the highest frequency occurring in colorectal cancer (>8% in two datasets, **Fig. 1A**). Importantly, over one-third of these defects were truncating alterations and 58% were missense mutations, with approximately half predicted to be deleterious by PolyPhen-2 (23), including alterations in the catalytic RASGAP and period-like domains. In total, 70% of the alterations in *DAB2IP* found in colorectal cancer are expected to be deleterious (**Fig. 1B**).

Nevertheless, because *DAB2IP* can be suppressed in breast cancer by epigenetic mechanisms (16), we also compared the methylation status of the *DAB2IP* promoter in 353 colorectal cancers and 32 normal adjacent colon tissues (18). Whereas none of the normal colon tissues exhibited methylation at the *DAB2IP* promoter, *DAB2IP* was selectively hypermethylated in 81.3% of the matched tumor samples (287/353; **Fig. 1C**). This finding was in stark contrast to 10 other RASGAP genes, which exhibited little or no promoter hypermethylation in colorectal cancers (**Fig. 1C**). Given that *DAB2IP* suppression triggers the aberrant activation of the RAS/ERK pathway, we expected that *DAB2IP* methylation might be enriched in tumors lacking *KRAS* or *BRAF* mutations. However, that was not the case; *DAB2IP* methylation frequently co-occurred with *KRAS* and *BRAF* alterations in colorectal cancers (**Fig. 1C**, top). In fact, *DAB2IP* was methylated in 78.8% of *KRAS* and 100% of *BRAF* mutant colorectal cancers.

Consistent with the observed hypermethylation of the *DAB2IP* promoter, *DAB2IP* mRNA levels were significantly lower in these tumors compared with normal tissue (**Fig. 1D**). We further confirmed that DAB2IP protein was absent or substantially reduced in multiple human colorectal cancer cell lines, including those with *KRAS* mutations (**Fig. 1E**). Of note, *DAB2IP* loss was not associated with or limited to any specific type of activating *KRAS* mutation (**Fig. 1F**). Altogether these findings reveal that *DAB2IP* is mutated or suppressed in a striking majority of colorectal cancers, including those harboring oncogenic *KRAS* mutations, suggesting that functions other than its GAP activity toward KRAS might be critical for tumor suppression in this tissue.

### *DAB2IP* loss exclusively promotes colorectal cancer growth *in vivo*

To investigate how DAB2IP functions in the context of colorectal cancer, we assessed the effects of *DAB2IP* suppression or reconstitution on cell proliferation, anchorage-independent growth, and tumor formation *in vivo* using two different models. Because the *DAB2IP* gene is expressed in HCT116 cells, *DAB2IP* was suppressed by shRNA sequences (**Fig. 2A**, left). Conversely, DLD-1 cells, which lack DAB2IP, were reconstituted with a *DAB2IP* cDNA (**Fig. 2B**, left). Unexpectedly, *DAB2IP* loss or reconstitution had no effect on cell proliferation *in vitro* or colony growth in soft agar, respectively (**Fig. 2A** and **B**). Strikingly however, *DAB2IP* did have a major effect on tumor growth *in vivo*. Whereas *DAB2IP* ablation potently enhanced the development of HCT116 xenografts (**Fig. 2C**), *DAB2IP* reconstitution suppressed the growth of DLD-1 tumors (**Fig. 2D**). Together, these observations demonstrate that *DAB2IP* can function as a tumor suppressor in colorectal cancers and does so by regulating biological processes that are uniquely important for tumor growth *in vivo*.

### DAB2IP's RASGAP activity on wild-type H- and N-RAS is required for its tumor suppressive function

DAB2IP functions as a tumor suppressor in prostate and breast cancers, two tumor types in which *RAS* mutations are rare, supporting the notion that DAB2IP inactivation provides an alternative means of activating the RAS pathway in these malignancies (16, 25). However, mutations in the RAS/ERK pathway are common in colorectal cancer. Moreover, *DAB2IP* is frequently suppressed or mutated in *KRAS* and *BRAF* mutant colorectal cancers, suggesting that these events are not redundant (**Fig. 1C**). Therefore, we investigated whether DAB2IP could affect RAS signaling in colorectal cancers. Surprisingly, *DAB2IP* reconstitution potently suppressed phospho-ERK and to a lesser extent phospho-AKT in DLD-1 cells, despite the presence of an activating *KRAS* mutation (**Fig. 2E**). Suppression was dependent on its RASGAP activity, as the GAP-deficient mutant, $DAB2IP^{R289L}$ (25), was unable to suppress these downstream effectors (**Fig. 2E**). Conversely, siRNA-mediated ablation of *DAB2IP* in HCT116 cells, which also harbor an oncogenic *KRAS* mutation, dramatically increased phospho-ERK and phospho-AKT levels (**Fig. 2F**, left). Together these observations unexpectedly demonstrate that *DAB2IP* loss has a major impact on RAS signaling in colorectal cancers, even in the presence of an activated *KRAS* allele, suggesting that DAB2IP plays an essential role in restraining ERK and AKT activity in this tissue, presumably through its effect on wild-type RAS proteins.

To investigate this possibility, RAS-GTP pull-down assays were performed to identify the RAS isoforms that were regulated by DAB2IP in this setting. *DAB2IP* ablation in HCT116 cells increased

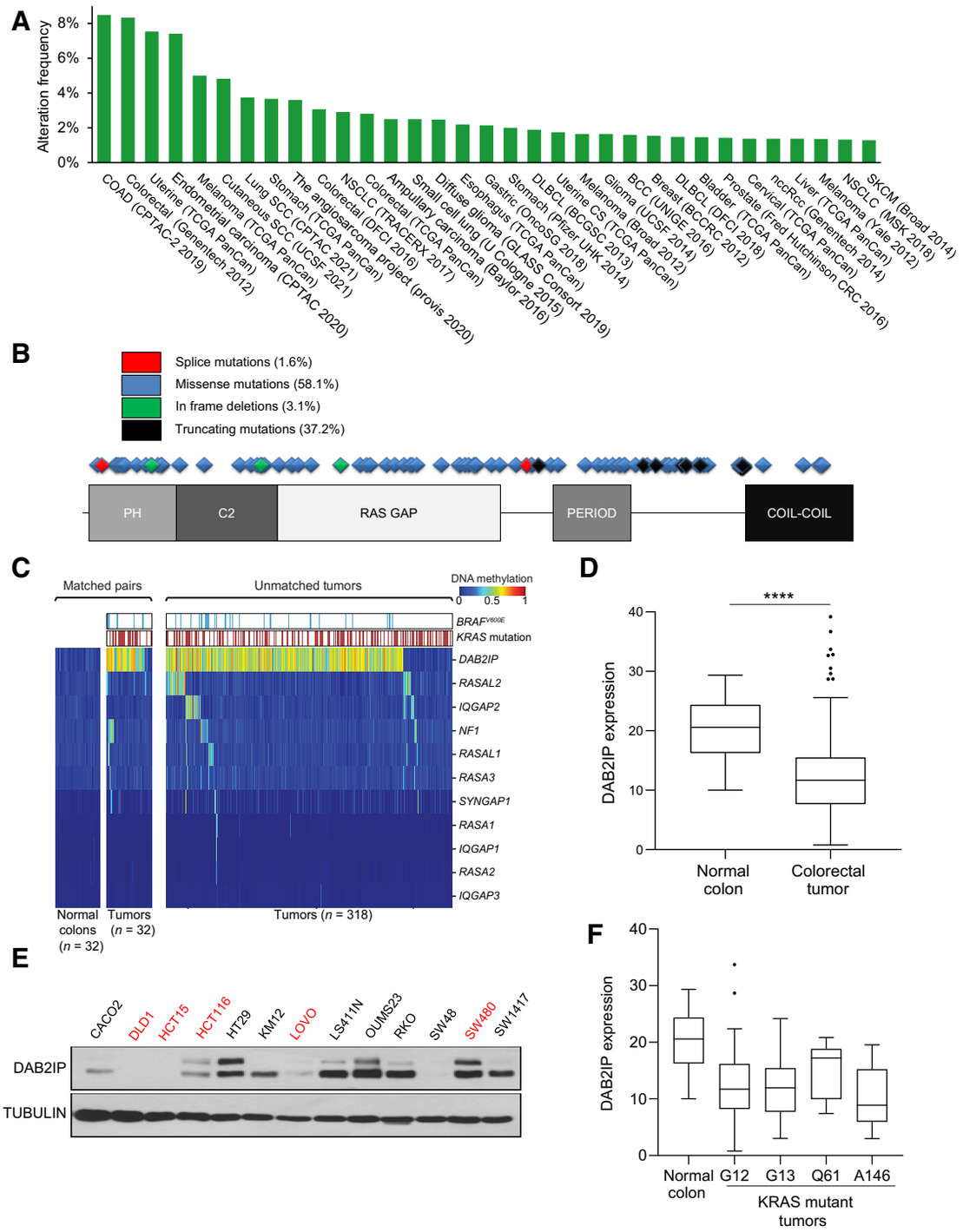


**Figure. 1.**

*DAB2IP* is frequently inactivated in human colorectal cancer via genetic and epigenetic mechanisms. **A,** Frequency of *DAB2IP* mutations in human tumors (retrieved in cBioPortal, restricted to studies of over 50 samples). **B,** Distribution of *DAB2IP* mutations in human colorectal cancer. Data was collected from cBioPortal and COSMIC. Splice mutations resulting in decreased expression are represented in red, missense mutations in blue, in frame deletions in green, and truncating mutations in black. **C,** Methylation data of RASGAP family members in 32 normal and 350 colon cancer samples. Four genes are not included: *RASA4* and *RASA4B* (masked promoter probes) and *RASAL3* and *PLXNB2* (methylated promoters in normal). KRAS (red) mutations are noted in corresponding patient samples. **D,** *DAB2IP* mRNA levels in normal colon and colon tumors from TCGA COAD. $^{****}$, $P = 2.9 \times 10^{-5}$, Wilcoxon rank sum test. The Tukey boxplot represents the interquartile range with the median line and outliers shown. **E,** DAB2IP protein levels in a panel of human colon cancer cell lines. *KRAS* mutant cell lines are shown in red. **F,** *DAB2IP* mRNA levels in normal colon and *KRAS* mutant *G12*, *G13, Q61,* and *A146* tumors from TCGA COAD. *G12*, *G13, Q61,* and *A146*, $P$ = ns, nonsignificant, ANOVA. The Tukey boxplot represents the interquartile range with the median line and outliers shown.

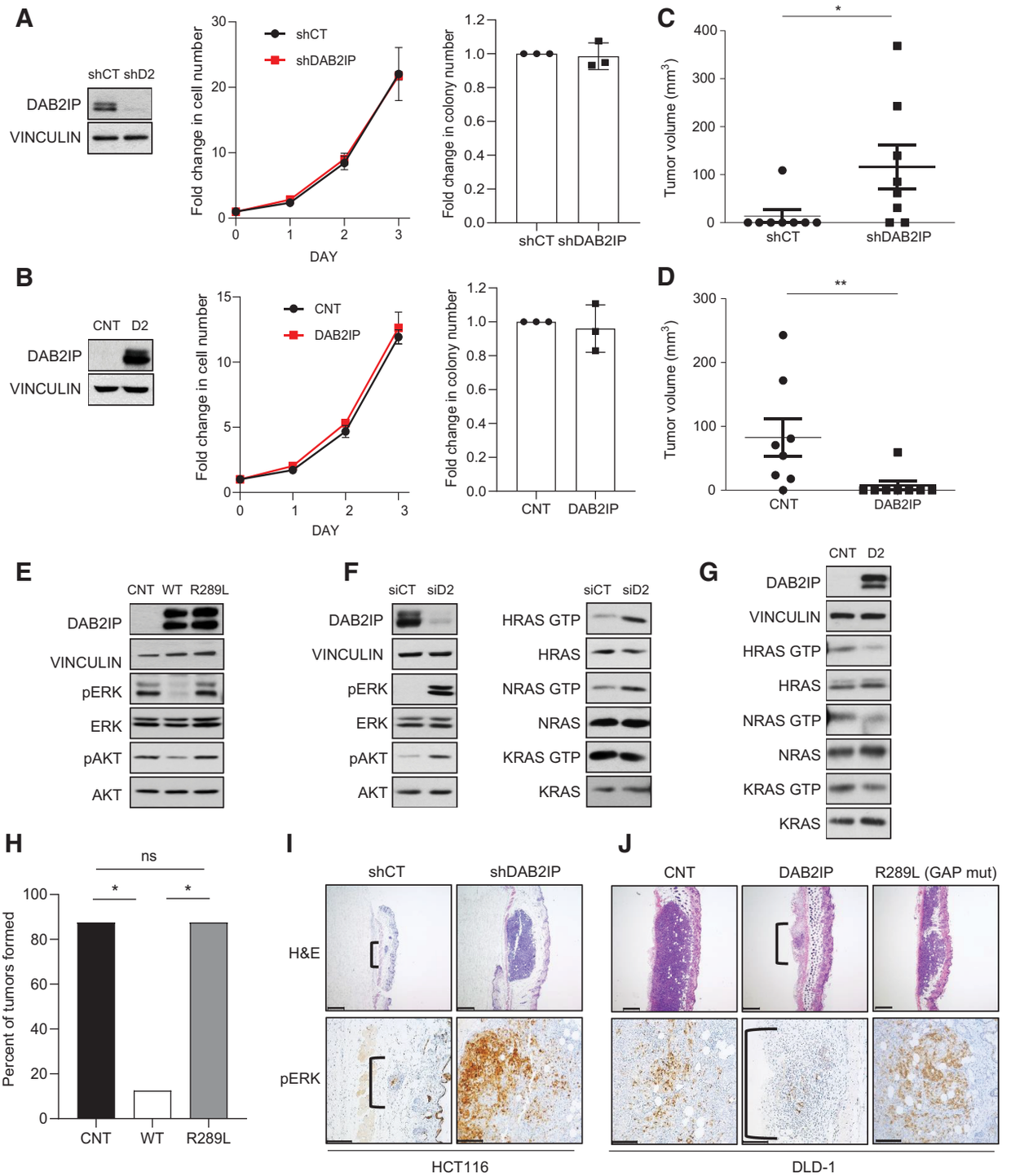


**Figure 2.**

DAB2IP functions as a tumor suppressor in colorectal cancer, in part, by regulating wild-type RAS proteins. **A,** HCT116 cells were transduced with a scrambled shRNA control (shCT) or a 3′ UTR shDAB2IP (shD2). Left, an immunoblot showing DAB2IP protein expression. Middle, graph of a cell proliferation assay depicting fold change in cell number after 3 days compared with day 0. Right, soft agar colony quantification showing fold change of colonies over the shCT control. $P$ = ns, nonsignificant, two-tailed $t$ test with Welch correction. **B,** DLD-1 cells expressing either control LACZ (CNT) or DAB2IP cDNA (D2). Left, an immunoblot showing DAB2IP protein expression. Middle, graph of a cell proliferation assay. Right, soft agar colony quantification. $P$ = ns, two-tailed $t$ test. **C,** Xenograft tumor formation of HCT116 cells expressing a DAB2IP shRNA compared with shCT ($n = 8$ per group). Tumor volumes were calculated at 2.5 weeks post injection ($n = 8$ per group). *, $P = 0.0238$, Mann–Whitney. The graphs represent mean ± SEM. (*Continued on the following page.*)

HRAS- and NRAS-GTP levels but did not further enhance KRAS activity, as would be expected in cells already harboring an activating *KRAS* mutation (**Fig. 2F**, right). Conversely, *DAB2IP* reconstitution in *KRAS* mutant DLD-1 cells reduced HRAS- and NRAS-GTP levels (**Fig. 2G**). Nevertheless, to determine whether the aberrant activation of these wild-type RAS proteins was required for tumor development, the consequences of reconstituting *DAB2IP*-deficient cells with wild-type or GAP-deficient $DAB2IP^{R289L}$ were assessed *in vivo*. Whereas wild-type DAB2IP potently suppressed tumor development, $DAB2IP^{R289L}$ was unable to do so (**Fig. 2H**). Histologic images of tumors described in **Fig. 2C**, **D**, and **H** further illustrate the profound effects that *DAB2IP* ablation and reconstitution have on tumor development and tumor suppression, respectively (**Fig. 2I** and **J**), as well as the defective tumor suppressor activity of $DAB2IP^{R289L}$ (**Fig. 2J**). IHC analysis of pERK in these tumors mirrored the pattern of activation/suppression observed *in vitro*, and also confirmed that $DAB2IP^{R289L}$ was unable to suppress RAS/ERK signaling *in vivo* (**Fig. 2I** and **J**). Together these studies demonstrate that DAB2IP critically regulates RAS signaling in colorectal cancer through its effects on HRAS and NRAS proteins, even in the presence of an oncogenic *KRAS* mutation, and that the aberrant activation of these wild-type proteins promotes the development of *DAB2IP*-deficient tumors.

### The period-like domain of DAB2IP and aberrant NF-κB activation are also important for colorectal cancer development

In addition to its RASGAP activity, DAB2IP also suppresses the NF-κB pathway through its period-like domain (25, 26). Given the importance of NF-κB in inducing and maintaining an inflammatory environment (27), we investigated whether *DAB2IP* loss might also be mediating its effects in colorectal cancer via NF-κB. If so, such a finding might help explain the discrepancy between *in vitro* and *in vivo* phenotypes, as growth *in vivo* is also influenced by the TME.

We first confirmed that genetic suppression of *DAB2IP* in HCT116 cells induced NF-κB activation, using a transcriptional reporter assay (**Fig. 3A**). Conversely, *DAB2IP* reconstitution in DLD-1 cells suppressed NF-κB activity (**Fig. 3B**). Importantly, *DAB2IP* suppression or reconstitution similarly activated/inhibited NF-κB and ERK in two additional colorectal cancer cell lines (**Fig. 3C** and **D**).

Consistent with these *in vitro* effects on NF-κB, ssGSEA of primary human tumors also revealed that NF-κB-regulated inflammatory gene signatures (HINATA_NFKB_IMMU_INF) are enriched in colon cancers with low levels of *DAB2IP* versus high levels of *DAB2IP* (**Fig. 3E**; ref. 20). To determine whether the induction of these genes might be a direct consequence of *DAB2IP* loss in cancer cells, RNA-seq analysis was performed in both the *DAB2IP* LOF (HCT116) and *DAB2IP* GOF (DLD-1) models. Indeed, these NF-κB–regulated inflammatory signatures were either upregulated or suppressed in cells where *DAB2IP* was ablated or reconstituted, respectively (**Fig. 3F** and **G**). Together, these observations suggest that *DAB2IP* loss in tumor cells is an important regulator of NF-κB and inflammatory signature genes in colorectal cancers.

To investigate whether NF-κB activation was playing a functional role in the development of *DAB2IP*-deficient tumors, we first assessed the effects of point mutations in either the period-like or GAP domain of *DAB2IP*. As expected, a *DAB2IP* allele containing a point mutation in the period-like domain ($DAB2IP^{S604A}$), which has previously been shown to be defective in its ability to inhibit NF-κB (25), failed to suppress NF-κB activity in DLD-1 cells (**Fig. 3H**). Interestingly however, the $DAB2IP^{R289L}$ RASGAP mutant was also unable to effectively suppress NF-κB, although defects were not as profound as with the $DAB2IP^{S604A}$ mutant (**Fig. 3H**). While these mutations have not previously been directly compared in this assay, these findings are consistent with the well-accepted paradigm that RAS activates the NF-κB pathway (6), and further suggest that DAB2IP may provide a direct molecular link between these two pathways. Regardless, these data demonstrate that DAB2IP must possess both an intact period-like and RASGAP domain to effectively suppress NF-κB, although the former may be slightly more important.

These *DAB2IP* point mutants along with the IκBα super repressor (*IκBαSR*; ref. 17), which blocks NF-κB activation, were then used to assess the functional requirement for NF-κB in the development of *DAB2IP*-deficient tumors. Similar to reconstitution with wild-type *DAB2IP*, $DAB2IP^{S604A}$, and $DAB2IP^{R289L}$ also had no effect on proliferation *in vitro* (**Fig. 3I**). The *IκBαSR*, which effectively inhibited NF-κB (**Fig. 3J**), also had no effect on proliferation (**Fig. 3K**). However, *in vivo* studies were more informative. Notably, both wild-type *DAB2IP* and the *IκBαSR*, inhibited tumor formation *in vivo* (**Fig. 3L**). By contrast, both the period-like domain mutation ($DAB2IP^{S604A}$), and the RASGAP mutant ($DAB2IP^{R289L}$), were equally defective in suppressing tumor development (**Fig. 3L**). Histologic images further illustrate the defective tumor suppressive activity of these mutant *DAB2IP* alleles (**Fig. 3M**). Notably, IHC staining of pERK in tumors confirmed that DAB2IP was able to suppress pERK and that the GAP mutant was unable to do so; however, the period-like domain mutant retained its ability to reduce ERK activation (**Fig. 3M**). Collectively these observations demonstrate that: (i) *DAB2IP* loss activates RAS and NF-κB, (ii) both the GAP domain and period-like domain are critical for its tumor suppressor activity, (iii) ultimately both domains impact NF-κB signaling, and (iv) DAB2IP's effects on NF-κB, through loss of both activities/domains are particularly important in/for colorectal cancer development. As shown in **Fig. 1B**, deleterious point mutations in both domains can be detected in human colorectal cancers.

### *DAB2IP* loss stimulates the production of inflammatory mediators and tumor development and can be suppressed by agents that block their expression

Consistent with its role in inflammation, many canonical NF-κB targets are cytokines/inflammatory mediators (28). However, NF-κB

(*Continued.*) **D,** Xenograft tumor formation in DLD-1 cells expressing LACZ (CNT) or DAB2IP cDNA. Tumor volumes were calculated at 3 weeks post injection ($n = 8$ per group). $^{**}$, $P = 0.005$ for DLD-1, Mann–Whitney. The graphs represent mean ± SEM. **E,** Western blot of total cell lysates from DLD-1 (KRAS mutant) cells stably infected with LACZ (CNT), DAB2IP (WT), and a GAP mutant (R289L) cDNA. **F,** DAB2IP knockdown in HCT116 (KRAS mutant) cells using a nonsilencing control (siCT) siRNA and siDAB2IP (siD2). Left, Western analysis showing DAB2IP loss results in an increase of pAKT and pERK. Right, a RAS activation assay measuring GTP bound Ras. **G,** Ras activation assay of DLD-1 cells infected with LACZ (CNT) and DAB2IP (D2) cDNA showing a decrease in H-RAS and N-RAS GTP levels in response to DAB2IP reconstitution. **H,** Bar graph depicting the percentage of tumors formed after injecting DLD-1 cells stably infected with LACZ (CNT), DAB2IP (WT), or a GAP mutant (R289L) cDNA into mice ($n = 8$ per group). The graph depicts the percentage of tumors that formed by 3 weeks. $^{*}$, $P = 0.01$ for CNT-WT and WT-R289L, Fisher exact test. **I** and **J,** Photographs of xenograft tumors. Sections were stained with hematoxylin and eosin (H&E; top) or pERK (bottom). Scale bar, 500 mm and 150 mm, respectively. **I,** HCT116 tumors expressing shCT or shDAB2IP at day 9 post injection are shown. The small shCT tumor is indicated with a bracket. **J,** DLD-1 tumors expressing CNT, DAB2IP, and R289L (GAP mut) at day 8 post injection are shown. The small DAB2IP tumor is indicated with a bracket.

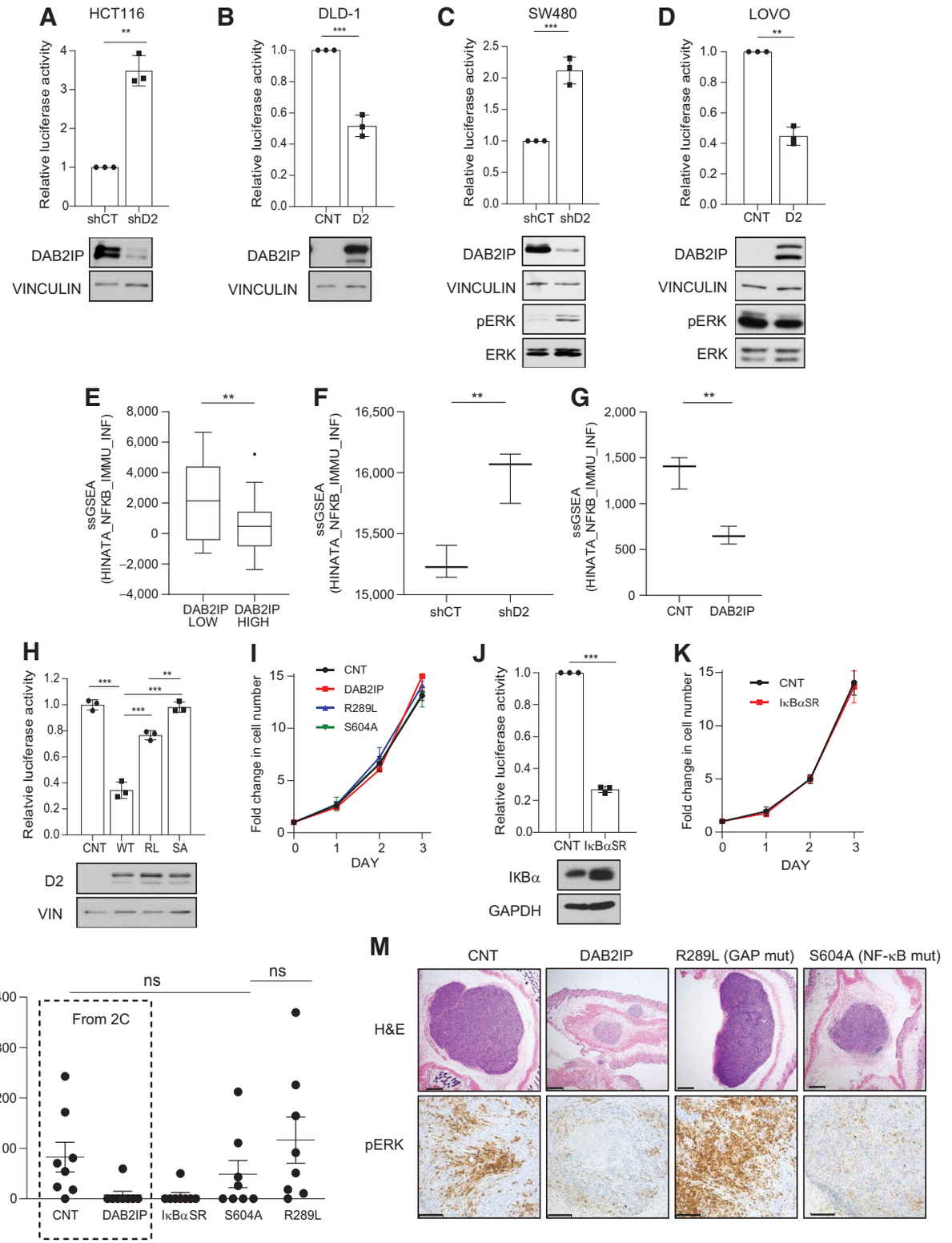
A
HCT116
Relative luciferase activity
shCT shD2
DAB2IP
VINCULIN
B
DLD-1
CNT D2
C
SW480
pERK
ERK
D
LOVO
E
ssGSEA (HINATA_NFKB_IMMU_INF)
DAB2IP LOW DAB2IP HIGH
F
shCT shD2
G
CNT DAB2IP
H
Relatvie luciferase activity
CNT WT RL SA
D2
VIN
I
Fold change in cell number
DAY
R289L
S604A
J
IKBα
GAPDH
K
IκBαSR
L
Tumor volume (mm3)
ns
From 2C
M
H&E
pERK
R289L (GAP mut)
S604A (NF-κB mut)

can also directly regulate prosurvival pathways in tumor cells (27). To determine which role might be more important, we first examined established prosurvival responses to NF-κB activation; however, we did not detect any increase in the expression of known proapoptotic effectors or a decrease in prosurvival effectors (Supplementary Fig. S1). Therefore, we investigated whether DAB2IP loss was stimulating the production of cytokines and/or other mediators of inflammation, which might then function by recruiting other protumorigenic cell types *in vivo*.

To identify potential DAB2IP-regulated mediators of inflammation we assessed the effects of *DAB2IP* ablation in HCT116 cells. While the expression of several cytokines and inflammatory mediators slightly increased, five stood out as they were induced 5- to 20-fold (**Fig. 4A**): specifically, IL8, CXCL1, PAI-1, IL32A, and ICAM-1. Conversely, we assessed changes in the expression of the same panel of proteins in DLD-1 cells −/+ DAB2IP reconstitution. In this model only a few inflammatory mediators were detected, however all four were among the same differentially expressed proteins identified in **Fig. 4A** (**Fig. 4B**). Notably, these factors were suppressed by DAB2IP reconstitution in this setting, albeit one was modestly reduced (**Fig. 4B**). Finally, we determined which inflammatory mediators were present in *DAB2IP*-deficient tumors *in vivo* and detected all five of the factors highlighted in **Fig. 4A**, although as expected many more were present *in vivo* (**Fig. 4C**).

Because multiple (i.e., five) tumor-derived cytokines/inflammatory mediators were induced by *DAB2IP*-loss, we exploited CYT-387 (Momelotinib), a compound that has been shown to broadly suppress cytokine production by inhibiting JAK1/2 and TBK1/IKKε kinases (29, 30). First, we confirmed that CYT-387 could suppress NF-κB activity in this model (**Fig. 4D**). Moreover, similar to the *IκBαSR*, it did not inhibit cell proliferation *in vitro* (**Fig. 4E**).

However, CYT-387 did suppress tumor development *in vivo* (**Fig. 4F**). Cytokine array analysis of a separate set of established tumors treated with CYT-387 for three days confirmed that CYT-387 could reduce the expression of these cytokines/inflammatory mediators *in vivo*, by ≈ 30% to 65% (**Fig. 4G**). However, while this experimental design was required to provide enough tissue for the comparison, it possibly underestimated the degree of inhibition due to the presence of inflammatory mediators prior to drug treatment. We attempted to ablate several of these cytokines and inflammatory mediators individually and assess tumor formation *in vivo*, however results were inconclusive because re-expressing tumors emerged and/or multiple cytokines may contribute to the response. Nevertheless, these observations are consistent with the hypothesis that the secretion of inflammatory mediators, induced by NF-κB, plays an important role in promoting the formation of *DAB2IP*-deficient tumors.

## Macrophage recruitment is important for the development of *DAB2IP*-deficient tumors

We therefore sought to determine whether *DAB2IP*-loss was indeed recruiting specific cells to tumors, and if so, assess their role in promoting tumor development. From the list of DAB2IP-regulated factors, we noted that many are involved in the recruitment, polarization, and/or activation of macrophages (31–34). Macrophages can play both tumorigenic and tumor suppressive roles in cancer. However, macrophages are associated with an increased risk of colorectal cancer development in the context of IBD (35, 36). Macrophages have also been shown to infiltrate early precancerous colonic lesions and polyps, further supporting a role for macrophages in colorectal cancer initiation (37). Consistent with a potential role for *DAB2IP* loss in colorectal cancer initiation, perhaps by promoting macrophage recruitment, mRNA expression analysis of human colorectal cancers revealed that *DAB2IP* is suppressed in the earliest stages of colon cancer development (TCGA COAD; **Fig. 5A**). ssGSEA analysis further demonstrated that tumor macrophage markers (20) are enriched in *DAB2IP* low versus *DAB2IP* high human colorectal cancer tissues (**Fig. 5B**).

To investigate whether macrophages might be promoting the development of *DAB2IP*-deficient tumors we first determined whether they were present in our models. Indeed, we found that macrophages were recruited at the earliest stages of tumor development and were readily detected within 4 days after injecting tumor cells (**Fig. 5C**). We then more carefully assessed their presence in all of our experimental models *in vivo*.

Strikingly, we observed macrophages infiltrating and scattered throughout the engineered *DAB2IP*-deficient tumors (HCT116), whereas DAB2IP expressing lesions were largely devoid of macrophages and, if present, were restricted to the periphery (**Fig. 5D**). Macrophages were also observed infiltrating *DAB2IP*-deficient DLD-1

**Figure. 3.**

The period-like domain and its effects on NF-kB are critical for DAB2IP's tumor suppressor function in colorectal cancer. **A–D,** Graphs depicting NF-κB activity using a luciferase reporter assay (top) and immunoblots (bottom) of total cell lysate. Activity is reported as the fold change of relative luciferase units. Two-tailed *t* test with Welch correction was performed. **A,** HCT116 cells expressing an shControl (shCT) or shDAB2IP (shD2). **, $P = 0.008$. **B,** DLD-1 cells expressing LACZ (CNT) or DAB2IP (D2) cDNA. ***, $P = 0.0003$. **C,** SW480 cells expressing an shControl (shCT) or shDAB2IP (shD2). ***, $P = 0.0008$. **D,** LOVO cells expressing LACZ (CNT) or DAB2IP (D2) cDNA. **, $P = 0.0038$. **E–G**, ssGSEA of mRNA using the gene set HINATA_NFKB_IMMU_INF (immune and inflammatory genes induced by NF-κB in keratinocytes). The Tukey boxplots represent the interquartile range with the median line and outliers shown. **E,** DAB2IP low compared with DAB2IP high tumor samples from colorectal adenocarcinoma TCGA PanCancer Atlas, $n = 30$ per group. **, $P = 0.005$, two-tailed *t* test with Welch correction. **F,** HCT116 cells expressing shControl (shCT) compared shDAB2IP (shD2). **, $P = 0.007$, unpaired *t* test. **G,** DLD-1 cells expressing LACZ (CNT) compared DAB2IP cDNA. **, $P = 0.004$, unpaired *t* test. **H,** NF-κB luciferase assay (top) and DAB2IP (D2) immunoblot (bottom) of DLD-1 cells expressing LACZ (CNT), DAB2IP (WT), R289L (RL), or S604A (SA). CNT vs. WT, ***, $P < 0.0001$; CNT vs. RL, **, $P = 0.001$; CNT vs. SA, $P =$ ns, nonsignificant; WT vs. RL, ***, $P < 0.0001$; WT vs. SA, ***, $P < 0.0001$; RL vs. SA, **, $P = 0.002$, ANOVA followed by Tukey multiple comparisons test. **I,** Graph depicting a cell proliferation assay comparing CNT, WT, RL, and SA in DLD-1 cells. The fold change in cell number after 3 days compared with day 0 was measured. **J,** Bar graph depicting activity from a NF-κB luciferase assay (top) and immunoblot (bottom) of DLD-1 cells comparing empty vector control (CNT) and the NF-κB inhibitor (IκBαSR) cDNA expression. ***, $P < 0.0001$, two-tailed *t* test with Welch correction. **K,** Graph depicting a cell proliferation assay of DLD-1 cells expressing empty vector Babe puro (CNT) or IκBα super repressor (IκBαSR). **L,** Dot plot depicting tumor size of DLD-1 xenografts derived from cells stably infected with LACZ (CNT), DAB2IP, IκBαSR, period-like domain mutant (S604A), and the GAP mutant (R289L; $n = 8$ per group). CNT and DAB2IP tumors were also shown in **Fig. 2C** and are included here for comparison. WT DAB2IP and IκBαSR inhibit tumor formation but LACZ, S604A, and R289L do not. Tumor volumes were measured at 3 weeks post injection. $P =$ ns for CNT-S604A and R289L-S604A, Mann–Whitney. The graph represents mean ± SEM. **M,** Photographs of DLD-1 xenograft tumors expressing CNT, DAB2IP, R289L (GAP mut), or S604A (NF-κB mut) at day 14 post injection. Sections were stained with hematoxylin and eosin (H&E; top) or pERK (bottom). Scale bar, 500 mm and 150 mm, respectively.

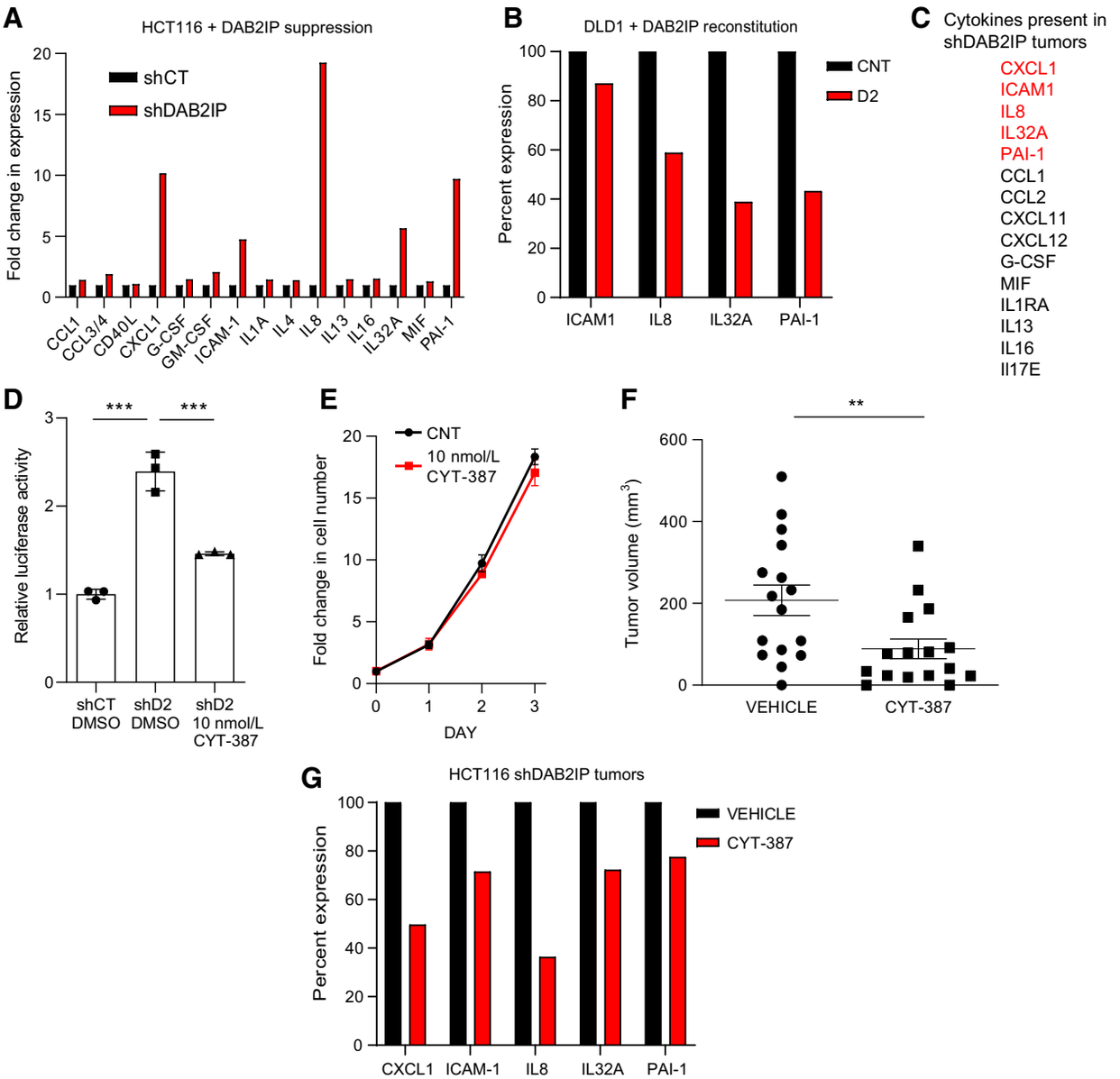


**Figure 4.**

DAB2IP-regulated cytokines/inflammatory mediators promote tumor formation. **A–C,** Cytokine immunoassays. Comparative protein levels were measured using ImageJ software. **A,** Graph of inflammatory mediators expressed and quantified from HCT116 shCT and shDAB2IP cell lysates. The graph depicts the fold change expression over shCT control. **B,** Graph depicting relative expression of ICAM-1, IL8, IL32A, and PAI-1 in CNT and DAB2IP (D2) cDNA expressing DLD-1 cells. Expression is measured as percent compared to shCT control. **C,** List of cytokines and inflammatory mediators detected in HCT116 tumors with DAB2IP suppression (shDAB2IP) using cytokine immunoassays. **D,** Graph depicting NF-κB activity as measured by a luciferase assay, comparing HCT116 shDAB2IP (shD2) cells treated with DMSO or 10 nmol/L CYT-387 for 16 hours. shCT DMSO was used as a control. Activity is reported as the fold change of relative luciferase units. shCT DMSO vs. shD2 DMSO, ***, $P < 0.0001$; shD2 DMSO vs. shD2 CYT, ***, $P < 0.0001$, ANOVA followed by Tukey multiple comparisons test. **E,** Graph of cell proliferation assay comparing shDAB2IP DMSO (CNT) and shDAB2IP 10 nmol/L CYT-387 in HCT116 cells. The fold change in cell number after 3 days compared with day 0 was measured. **F,** Dot plot depicting tumor size of shDAB2IP HCT116 xenografts −/+ CYT-387. Mice were pretreated daily 3 days prior to injection and then daily with 50 mg/kg CYT-387 or vehicle ($n = 16$ each). Volume of tumors was calculated 2.5 weeks after injection. **, $P = 0.0095$, Mann–Whitney. The graphs represent mean ± SEM. **G,** Graph depicting cytokine and inflammatory mediator expression levels, as measured by cytokine arrays, in the presence and absence of CYT-387 *in vivo*. Established HCT116 shDAB2IP tumors were treated daily for 3 days with 50 mg/kg of CYT-387 or vehicle. Percent expression is graphed.

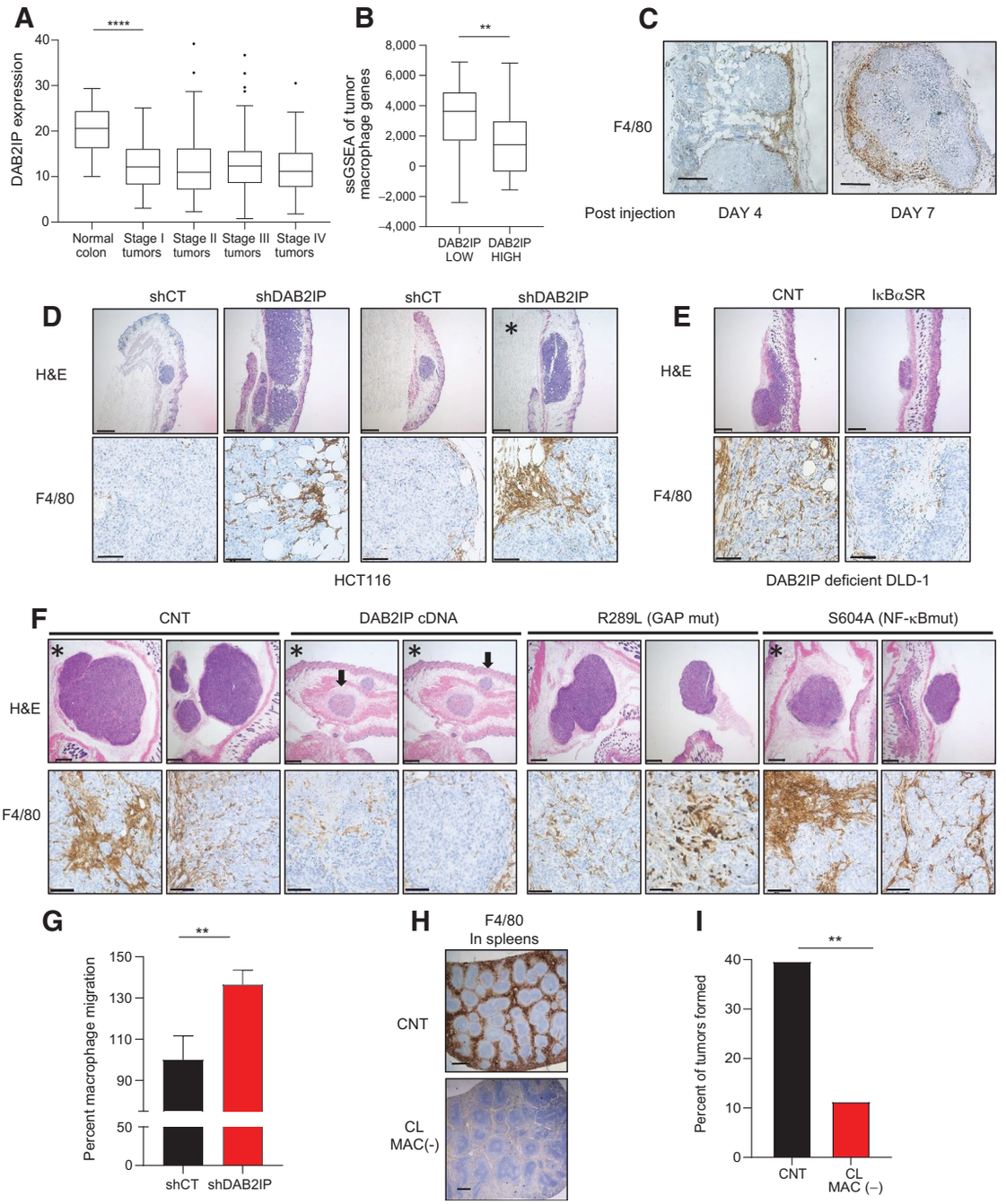


**Figure. 5.**

Macrophages are rapidly recruited to shDAB2IP tumors and contribute to their development. **A,** Graph depicting DAB2IP mRNA levels in normal colon, stages I–IV colon cancer, or undesignated colon cancer samples from TCGA COAD. ****, $P = 4.36 \times 10^{-9}$ (normal vs. stage I), Wilcoxon rank sum test. Stage I, stage II, stage III, stage IV compared with each other. $P$ = ns, nonsignificant, ANOVA. The Tukey boxplot represents the interquartile range with the median line and outliers shown. **B,** Boxplot of ssGSEA comparing DAB2IP low and high samples from colorectal adenocarcinoma TCGA PanCancer Atlas, $n = 30$ per group. Using a tumor macrophage gene set (Supplementary Table S2; ref. 20), DAB2IP low tumors are enriched for macrophage markers. **, $P = 0.0065$, two-tailed $t$ test with Welch correction. The Tukey boxplot represents the interquartile range with the median line shown. **C,** IHC images of shDAB2IP HCT116 tumor sections at day 4 and 7 post cell injection. Macrophages were stained using F4/80. Scale bar, 200 mm. **D–F,** IHC images of xenograft tumors. Sections were stained with hematoxylin and eosin (H&E; top) or F4/80 (bottom). Scale bar, 500 mm and 75 mm, respectively. **D,** HCT116 tumors expressing shCT control or shDAB2IP at 8 days (left) and 9 days (right) post injection. * indicates the same tumor was stained for pERK in **Fig. 2I**. **E,** DLD-1 tumors expressing empty control vector (CNT) or IκBαSR at day 8 post injection. **F,** DLD-1 tumors expressing LACZ (CNT), DAB2IP, R289L, or S604A cDNA 14 days post injection. Arrows, DAB2IP tumors. * indicates the same tumors were stained for pERK in **Fig. 3M**. **G,** Graph quantifying results from a transwell migration assay comparing the effect of conditioned media from shControl (shCT) shDAB2IP HCT116 cells and cells on the induction of migration by RAW264.7 macrophages. Percent of migration of macrophages is plotted. **, $P = 0.0098$, two-tailed $t$ test. **H,** IHC images of mouse spleens treated twice with 1 mg/mL Encapsome (CNT) or Clodrosome. Macrophages were stained using F4/80. Scale bar, 500 mm. **I,** Graph depicting inhibition of xenograft tumor formation using shDAB2IP HCT116 cells. Mice were pretreated once with 1 mg Encapsome (CNT) or Clodrosome (CL MAC-) 3 days prior to injection and then every 3 days ($n = 38$ CNT; $n = 36$ Clodrosome). Percent of tumors formed at day 7 is graphed. **, $P = 0.0073$, Fisher exact test.

tumors and importantly, this was prevented by the expression of the *IκBαSR* (**Fig. 5E**). These results suggest that *DAB2IP* loss in tumor cells promotes the recruitment and infiltration of macrophages and that this is dependent on the activation of NF-κB.

Next, we investigated how the expression wild-type and mutant *DAB2IP* alleles affected macrophage infiltration. While macrophages were readily detected infiltrating *DAB2IP*-deficient tumors (**Fig. 5D** and **F**), *DAB2IP* reconstitution prevented this robust infiltration (**Fig. 5F**). Notably, $DAB2IP^{S604A}$, which was completely defective in its ability to inhibit NF-κB, was also unable to prevent the infiltration of macrophages, which were observed throughout these tumors (**Fig. 5F**). Macrophages were also readily detected in tumors expressing the GAP domain mutant, $DAB2IP^{R289L}$, however infiltration appeared to be more pronounced in the $DAB2IP^{S604A}$ mutant, consistent with the slightly higher NF-κB activity in these reconstituted cells (**Figs. 5F** and **3B**).

In support of the notion that *DAB2IP* suppression was triggering the release of several factors that can recruit macrophages to a developing tumor, we found that media from *DAB2IP*-deficient tumor cells promoted the migration/chemotaxis of RAW264.7 macrophages *in vitro*, as compared with media from control cells (**Fig. 5G**). However, to assess the functional contribution of macrophages to tumor development *in vivo*, macrophages were eliminated in mice by treating them with liposomal clodronate (Clodrosome; ref. 38). Notably, macrophages were effectively depleted in these animals, as confirmed by their absence in the spleen (**Fig. 5H**). More importantly however, Clodrosome treatment suppressed the formation of *DAB2IP*-deficient tumors (**Fig. 5I**). Thus, in addition to affecting RAS signaling, these data demonstrate that DAB2IP loss triggers the potent activation of NF-κB, the release of cytokines/inflammatory mediators, and the subsequent recruitment of macrophages, which play an important role in the development of *DAB2IP*-deficient colorectal cancers.

## Discussion

The aberrant activation of the RAS pathway and cytokine-driven inflammatory cascades are two important events that drive colorectal tumor development. In this study we show that epigenetic or genetic inactivation of the tumor suppressor, *DAB2IP*, represents a strikingly common mechanism of simultaneously amplifying/activating both of these pathways in colorectal cancer. This is due to the fact that DAB2IP is a bifunctional tumor suppressor and regulates each signal via distinct domains. We further demonstrate that *DAB2IP* is lost early in colorectal cancer development and frequently co-occurs with *KRAS* and *BRAF* mutations. Thus, despite its RASGAP function, *DAB2IP* loss provides signals that are not redundant with, but instead cooperative with, mutations in *KRAS*.

Surprisingly, we show that *DAB2IP* loss has a major impact on RAS signaling in *KRAS* mutant tumors and substantially amplifies ERK and AKT signals by activating wild-type H- and N-RAS proteins. These effects are critical in colorectal cancers, as a GAP-deficient point mutant of *DAB2IP* fails to suppress tumor development. It should be noted that the role of other wild-type RAS proteins in *KRAS* mutant tumors has been somewhat controversial. For example, in some settings *KRAS* mutant tumors have been shown to require intact H- and/or N-RAS proteins for proliferation, growth, or survival (39–42), whereas in other studies the loss of wild-type *H*- or N-RAS enhanced *KRAS* tumor development (43, 44). However, these differences appear to be related to the requirement for specific levels of RAS activation in different tissues or at early versus later stages of development (45). Considered in this context, our findings suggest that colorectal cancers tolerate and benefit from higher levels of RAS pathway activation conferred by *DAB2IP* loss, and do so even at early stages of development, when *DAB2IP* loss occurs. It is also possible that *DAB2IP* loss may amplify signals from specific growth factor receptors in colorectal cancer, through its effects on wild-type RAS proteins, which is not a mutually exclusive concept. Regardless, these findings support the growing notion that effective colorectal cancer treatments may ultimately require suppression of both mutant and wild-type RAS proteins.

However, our data suggest that the selection for *DAB2IP* loss early in colorectal cancer development may be even more driven by its cancer-cell autonomous effects on cytokine/inflammatory mediator production and the recruitment of macrophages, through its effects on NF-κB. In fact, we found that both the RASGAP domain and the period-like domain ultimately regulate NF-κB and macrophage recruitment. While chronic inflammation is an important risk factor for colorectal cancers, inflammation also plays a role in the development and progression of spontaneous colorectal cancers, which represent the vast majority of cases (28). Nevertheless, little is known about how genetic or epigenetic alterations in cancer cells may directly initiate this response. Importantly, we showed that *DAB2IP* loss in tumor cells triggered the production of multiple inflammatory mediators and the recruitment of macrophages, which were required for tumor development *in vivo*. While we were not able to examine the contribution of T cells or the broader inflammatory process in this model, the rapid recruitment of macrophages is consistent with their proposed protumorigenic role in colorectal cancer and their presence in early colonic lesions. Moreover, given the well-established positive feedback loops between cytokines, NF-κB, and various cell types within colorectal cancers, the aberrant activation of NF-κB in tumor cells would be expected to have a major effect on both initiating and amplifying inflammatory cascades. Analysis of human tumors further revealed an association between low *DAB2IP* levels, macrophage markers, and NF-κB inflammatory signatures, consistent with the notion that DAB2IP loss promotes this process. Thus, these observations mirror important aspects of human colorectal cancer.

Collectively, these findings demonstrate that *DAB2IP*-loss plays a major and unappreciated role in substantially amplifying RAS signaling, triggering cytokine/inflammatory mediator production, and recruiting macrophages in colorectal cancer, all of which are critical for their development. The high frequency of *DAB2IP* loss in early-stage tumors further suggests that it normally functions as an important gatekeeper of these oncogenic pathways in this tissue.

### Authors' Disclosures

A.L. Miller reports grants from NCI during the conduct of the study. P.W. Laird serves on the scientific advisory boards of AnchorDx and of FOXO Technologies, which have an interest in DNA methylation-based diagnostics. This manuscript describes DNA methylation of DAB2IP in colorectal cancer. K. Cichowski reports personal fees from Erasca outside the submitted work. No disclosures were reported by the other authors.

### Authors' Contributions

**A.L. Miller:** Conceptualization, investigation, methodology, writing–original draft, writing–review and editing. **N. Perurena:** Formal analysis, visualization, writing–original draft, writing–review and editing. **A. Gardner:** Investigation. **T. Hinoue:** Formal analysis, investigation, methodology. **P. Loi:** Formal analysis. **P.W. Laird:**

Funding acquisition, methodology. **K. Cichowski:** Conceptualization, funding acquisition, methodology, writing–original draft, writing–review and editing.

## Acknowledgments

The authors acknowledge the Dana-Farber/Harvard Cancer Center in Boston, MA, for the use of the Specialized Histopathology Core, which provided histology and IHC service. Dana-Farber/Harvard Cancer Center is supported in part by an NCI Cancer Center Support grant # NIH 5 P30 CA06516. This work was supported by the NCI RO1CA188659 and RO1CA111754 (to K. Cichowski).

The publication costs of this article were defrayed in part by the payment of publication fees. Therefore, and solely to indicate this fact, this article is hereby marked "advertisement" in accordance with 18 USC section 1734.

## Note

Supplementary data for this article are available at Cancer Research Online (http://cancerres.aacrjournals.org/).

Received February 1, 2022; revised February 1, 2023; accepted March 15, 2023; published first March 20, 2023.

## References

1. Cox AD, Fesik SW, Kimmelman AC, Luo J, Der CJ. Drugging the undruggable RAS: mission possible? Nat Rev Drug Discov 2014;13:828–51.
2. Hardiman KM. Update on sporadic colorectal cancer genetics. Clin Colon Rectal Surg 2018;31:147–52.
3. Vogelstein B, Fearon ER, Hamilton SR, Kern SE, Preisinger AC, Leppert M, et al. Genetic alterations during colorectal-tumor development. N Engl J Med 1988; 319:525–32.
4. Janssen KP, Alberici P, Fsihi H, Gaspar C, Breukel C, Franken P, et al. APC and oncogenic KRAS are synergistic in enhancing Wnt signaling in intestinal tumor formation and progression. Gastroenterology 2006;131: 1096–109.
5. Sansom OJ, Meniel V, Wilkins JA, Cole AM, Oien KA, Marsh V, et al. Loss of APC induces polyploidy as a result of a combination of defects in mitosis and apoptosis Proc Natl Acad Sci 2006;103:14122.
6. Chan TL, Zhao W, Leung SY, Yuen ST. BRAF and KRAS mutations in colorectal hyperplastic polyps and serrated adenomas. Cancer Res 2003;63: 4878–81.
7. Leach JDG, Vlahov N, Tsantoulis P, Ridgway RA, Flanagan DJ, Gilroy K, et al. Oncogenic BRAF, unrestrained by TGFβ-receptor signaling, drives right-sided colonic tumorigenesis. Nat Commun 2021;12:3464.
8. Schmitt M, Greten FR. The inflammatory pathogenesis of colorectal cancer. Nat Rev Immunol 2021;21:653–67.
9. Viennois E, Chen F, Merlin D. NF-κB pathway in colitis-associated cancers. Transl Gastrointest Cancer 2013;2:21–9.
10. Chan AT, Ogino S, Fuchs CS. Aspirin and the risk of colorectal cancer in relation to the expression of COX-2. N Engl J Med 2007;356:2131–42.
11. Flossmann E, Rothwell PM. Effect of aspirin on long-term risk of colorectal cancer: consistent evidence from randomized and observational studies. Lancet 2007;369:1603–13.
12. Klampfer L. Cytokines, inflammation and colon cancer. Curr Cancer Drug Targets 2011;11:451–64.
13. Grivennikov SI, Wang K, Mucida D, Stewart CA, Schnabl B, Jauch D, et al. Adenoma-linked barrier defects and microbial products drive IL23/IL17-mediated tumor growth. Nature 2012;491:254–8.
14. Schwitalla S, Ziegler PK, Horst D, Becker V, Kerle I, Begus-Nahrmann Y, et al. Loss of p53 in enterocytes generates an inflammatory microenvironment enabling invasion and lymph node metastasis of carcinogen-induced colorectal tumors. Cancer Cell 2013;23:93–106.
15. Simanshu DK, Nissley DV, McCormick F. RAS proteins and their regulators in human disease. Cell 2017;170:17–33.
16. Olsen SN, Wronski A, Castaño Z, Dake B, Malone C, De Raedt T, et al. Loss of RasGAP tumor suppressors underlies the aggressive nature of luminal B breast cancers. Cancer Discov 2017;7:202–17.
17. Boehm JS, Zhao JJ, Yao J, Kim SY, Firestein R, Dunn IF, et al. Integrative genomic approaches identify IKBKE as a breast cancer oncogene. Cell 2007; 129:1065–79.
18. Liu Y, Sethi NS, Hinoue T, Schneider BG, Cherniack AD, Sanchez-Vega F, et al. Comparative molecular analysis of gastrointestinal adenocarcinomas. Cancer Cell 2018;33:721–35.
19. Hinata K, Gervin AM, Jennifer Zhang Y, Khavari PA. Divergent gene regulation and growth effects by NF-kappa B in epithelial and mesenchymal cells of human skin. Oncogene 2003;22:1955–64.
20. Bindea G, Mlecnik B, Tosolini M, Kirilovsky A, Waldner M, Obenauf AC, et al. Spatiotemporal dynamics of intratumoral immune cells reveal the immune landscape in human cancer. Immunity 2013;39:782–95.
21. Zhou W, Laird PW, Shen H. Comprehensive characterization, annotation and innovative use of Infinium DNA methylation BeadChip probes. Nucleic Acids Res 2017;45:e22.
22. Ellrott K, Bailey MH, Saksena G, Covington KR, Kandoth C, Stewart C, et al. Scalable open science approach for mutation calling of tumor exomes using multiple genomic pipelines. Cell Syst 2018;6:271–81.
23. Adzhubei I, Jordan DM, Sunyaev SR. Predicting functional effect of human missense mutations using PolyPhen-2. Curr Protoc Hum Genet 2013;Chapter 7: Unit7.20.
24. McLaughlin SK, Olsen SN, Dake B, De Raedt T, Lim E, Bronson RT, et al. The RasGAP gene, RASAL2, is a tumor and metastasis suppressor. Cancer Cell 2013; 24:365–78.
25. Min J, Zaslavsky A, Fedele G, McLaughlin SK, Reczek EE, De Raedt T, et al. An oncogene-tumor suppressor cascade drives metastatic prostate cancer by coordinately activating Ras and nuclear factor-kappaB. Nat Med 2010;16: 286–94.
26. Zhang H, Zhang R, Luo Y, D'Alessio A, Pober JS, Min W. AIP1/DAB2IP, a novel member of the Ras-GAP family, transduces TRAF2-induced ASK1-JNK activation. J Biol Chem 2004;279:44955–65.
27. Xia Y, Shen S, Verma IM. NF-κB, an active player in human cancers. Cancer Immunol Res 2014;2:823–30.
28. Taniguchi K, Karin M. NF-κB, inflammation, immunity and cancer: coming of age. Nat Rev Immunol 2018;18:309–24.
29. Zhu Z, Aref AR, Cohoon TJ, Barbie TU, Imamura Y, Yang S, et al. Inhibition of KRAS-driven tumorigenicity by interruption of an autocrine cytokine circuit. Cancer Discov 2014;4:452–65.
30. Barbie TU, Alexe G, Aref AR, Li S, Zhu Z, Zhang X, et al. Targeting an IKBKE cytokine network impairs triple-negative breast cancer growth. J Clin Invest 2014;124:5411–23.
31. Vilgelm AE, Richmond A. Chemokines modulate immune surveillance in tumorigenesis, metastasis, and response to immunotherapy. Front Immunol 2019;10:333.
32. Gerszten RE, Garcia-Zepeda EA, Lim YC, Yoshida M, Ding HA, Gimbrone MA Jr., et al. MCP-1 and IL8 trigger firm adhesion of monocytes to vascular endothelium under flow conditions. Nature 1999;398:718–23.
33. Sun Y, Qian Y, Chen C, Wang H, Zhou X, Zhai W, et al. Extracellular vesicle IL32 promotes the M2 macrophage polarization and metastasis of esophageal squamous cell carcinoma via FAK/STAT3 pathway. J Exp Clin Cancer Res 2022; 41:145.
34. Kubala MH, Punj V, Placencio-Hickok VR, Fang H, Fernandez GE, Sposto R, et al. Plasminogen activator inhibitor-1 promotes the recruitment and polarization of macrophages in cancer. Cell Rep 2018;25:2177–91.
35. Erreni M, Mantovani A, Allavena P. Tumor-associated macrophages (TAM) and inflammation in colorectal cancer. Cancer Microenviron 2011;4:141–54.
36. Wang X, Huycke MM. Colorectal cancer: role of commensal bacteria and bystander effects. Gut microbes 2015;6:370–6.
37. McLean MH, Murray GI, Stewart KN, Norrie G, Mayer C, Hold GL, et al. The inflammatory microenvironment in colorectal neoplasia. PLoS One 2011;6: e15366.
38. Van Rooijen N, Sanders A. Liposome mediated depletion of macrophages: mechanism of action, preparation of liposomes, and applications. J Immunol Methods 1994;174:83–93.
39. Young A, Lou D, McCormick F. Oncogenic and wild-type Ras play divergent roles in the regulation of mitogen-activated protein kinase signaling. Cancer Discov 2013;3:112–23.

40. Jeng HH, Taylor LJ, Bar-Sagi D. Sos-mediated cross-activation of wild-type Ras by oncogenic Ras is essential for tumorigenesis. Nat Commun 2012;3: 1168.
41. Grabocka E, Pylayeva-Gupta Y, Jones MJ, Lubkov V, Yemanaberhan E, Taylor L, et al. Wild-type H- and N-Ras promote mutant K-Ras–driven tumorigenesis by modulating the DNA damage response. Cancer Cell 2014; 25:243–56.
42. Lim KH, Ancrile BB, Kashatus DF, Counter CM. Tumor maintenance is mediated by eNOS. Nature 2008;452:646–9.
43. Weyandt JD, Lampson BL, Tang S, Mastrodomenico M, Cardona DM, Counter CM. Wild-type Hras suppresses the earliest stages of tumorigenesis in a genetically engineered mouse model of pancreatic cancer. PLoS One 2015;10: e0140253.
44. To MD, Rosario RD, Westcott PM, Banta KL, Balmain A. Interactions between wild-type and mutant Ras genes in lung and skin carcinogenesis. Oncogene 2013; 32:4028–33.
45. Li S, Balmain A, Counter CM. A model for RAS mutation patterns in cancers: finding the sweet spot. Nat Rev Cancer 2018;18:767–77.